FILE

James Rennell Centre
for Ocean Circulation

INTERNAL DOCUMENT No. 23

Relationship between remotely-sensed signatures of the ocean and subsurface structure

P G Challenor, D Cromwell, T N Forrester,
T H Guymer & M S Jones

1995

UK
WOCE

Institute of
Oceanographic Sciences
Deacon Laboratory

Natural Environment Research Council

JAMES RENNELL CENTRE FOR OCEAN CIRCULATION

INTERNAL DOCUMENT No. 23

Relationship between remotely-sensed signatures of the ocean and subsurface structure

P G Challenor, D Cromwell, T N Forrester, T H Guymer & M S Jones

1995

Gamma House
Chilworth Research Park
Chilworth
Southampton SO1 7NS
Tel 01703 766184
Telefax 01703 767507

DOCUMENT DATA SHEET

AUTHOR
CHALLENOR, P G, CROMWELL, D, FORRESTER, T N, GUYMER, T H & JONES, M S

PUBLICATION DATE 1995

TITLE

Relationship between remotely-sensed signatures of the ocean and subsurface structure.

REFERENCE

James Rennell Centre for Ocean Circulation, Internal Document, No. 23, 32pp.
(Unpublished manuscript)

ABSTRACT

This is the first progress report under a Joint Research Council/Ministry of Defence research project on the relationship between remotely-sensed ocean signatures and subsurface structure and dynamics. It comprises an inventory of datasets and progress reports on sub-projects utilising *in situ*, altimetric and infrared data.

KEYWORDS

ALTIMETRY
ATLANTIC OCEAN
AZORES CURRENT
DRAKE PASSAGE
INFRARED
OCEAN SURFACE SIGNATURES
REMOTE SENSING
SEA SURFACE HEIGHT
SEA SURFACE TEMPERATURE
SUBSURFACE DYNAMICS

ISSUING ORGANISATION

Institute of Oceanographic Sciences
Deacon Laboratory
Wormley, Godalming
Surrey GU8 5UB. UK.

Director: Colin Summerhayes DSc

Telephone Wormley (0428) 684141
Telex 858833 OCEANS G.
Facsimile (0428) 683066

Copies of this report are available from: **The Library,** *PRICE*

CONTENTS PAGE

CHAPTER 1. INTRODUCTION

One of the major problems facing the satellite oceanographer is whether remotely-sensed data from the ocean surface contain any information about what is happening at depth. A key issue is the synergistic use of satellite and *in situ* data. However, the relationship between remotely-sensed signatures of the surface and subsurface features is not well understood. Consequently, it is not clear how effectively satellites can provide information on dynamically important aspects of the ocean. If it can be shown that there is information about subsurface ocean structure in the satellite data the question then arises as to how this can best be inferred from surface measurements.

A Joint Research Council/Ministry of Defence Research Grant was awarded with the project being defined by the following three aims (or sub-projects):

(1) To determine the relationship of surface remotely-sensed signatures on a variety of space scales to subsurface structure under different oceanographic and meteorological conditions;

(2) To develop techniques for combining remotely sensed and hydrographic data to yield improved estimates of subsurface structure and circulation;

(3) To assess the feasibility of inferring aspects of subsurface structure from remote sensing data in the absence of coincident *in situ* data.

A kick-off meeting with the Contract Officer, Dr J C Scott (DRA Portland), was held on 12 January 1994, jointly with a progress meeting for a Feature Modelling contract. The present document constitutes the first progress report and describes the progress made so far in relation to the objectives and deliverables of the project. We summarise the various datasets acquired to date and provide a preliminary assessment of priorities for analysis in relation to the proposed objectives and taking account (where possible) of data quality. It also presents some preliminary analyses using the datasets. A more detailed inventory of the *in situ* and satellite data acquired so far has been produced. This document will be continuously updated as further information becomes available; copies will be distributed on request.

CHAPTER 2. INVENTORY OF DATASETS

2.1 Inventory of *in situ* data

James Rennell Centre staff have participated in several cruises in the North Atlantic and Southern Ocean for which there also exists satellite data. Appendix B provides a brief overview of the cruise data sets which are most likely to be of value in our study. We have included two recent cruises, A23 in the South Atlantic, and SWINDEX II, in the South West Indian Ocean. SWINDEX II included segments along satellite ground tracks thus facilitating, for example, investigation of the temporal and spatial variability of absolute surface currents (see sections below on the Drake Passage and the Azores).

High accuracy Acoustic Doppler Current Profiler (ADCP) absolute velocity measurements, which are sensitive to errors in ship gyro error and ship position, are essential for this type of work. In this respect, the recent James Clark Ross survey in the Drake Passage, utilising an Ashtech GPS3DF receiver (giving ship's heading to 0.1 degree accuracy) and differential GPS (giving ship's position to 4 m accuracy at 1800 km from a static base station) is highly encouraging (King and Alderson, 1994).

Appendix B includes data collected in regions of strong baroclinic signal, e.g. CD51, around the Iceland-Faeroes Front, as well as more quiescent areas, e.g. CONVEX, which has already been successfully subjected to analysis by inverse techniques (Bacon, 1994). Several cruises have carried both SeaSoar and ADCP instrumentation, providing high resolution hydrographic data of the upper 500m of the ocean with horizontal resolution of a few kilometres. Such data can be synergistically combined with satellite altimeter measurements which have a comparable horizontal resolution of ~7 km. On the other hand, study of deeper oceanic structure below the thermocline requires the use of XBT's and CTD casts. In the latter case, horizontal resolution is then typically of 50-100 km and the question of how best to combine such hydrographic data with high (horizontal) resolution altimeter data is problematic. Additionally, caution should be exercised when CTD sections exceed several hundred km in length: in contrast to satellite observations, the data may no longer be approximately synoptic in areas where ocean features, specifically eddies and fronts, evolve rapidly in time.

2.2 Infrared data from satellites

Satellite infrared (IR) data held at the JRC comes from either the Advanced Very High Resolution Radiometer (AVHRR) or from the Along Track scanning Radiometer (ATSR). Data from both instruments are held in high and low spatial resolution. Most of the high resolution data are held on exabyte tapes.

ATSR Data

At present all the ATSR data held at JRC has been processed at the Rutherford Appleton Laboratory (RAL), and all useful data is in the latest RAL release version SADIST 500 (Synthesis of ATSR Data Into Sea-surface Temperatures). It is expected that with the recent launch of ERS-2 in April 1995, data from the new Advanced Along Track Scanning Radiometer (ATSR-2) will be in version SADIST 600. A copy of the SADIST format document may be obtained from RAL. ERS-1 was launched in July 1991 and much of the data observed before October 1991 is of poor quality and has not yet been reprocessed by RAL. Details of ATSR characteristics and data processing schemes are given in (Zavody *et al.*, 1994).

High Spatial Resolution Data

The high spatial resolution ATSR data comes in the form of 512 by 512 pixel image products, representing a 512 km^2 region. Each 1 km^2 pixel represents an interpolation of the forward and nadir view (if both are present) and an integration of the Instantaneous Field of View (IFOV) for either both or one view, which is most cases is larger than 1 km^2. The most useful data held at JRC for this project are the Sea Surface Temperature (SST) and Brightness Temperature (BT) level 2 products. The level 1 "counts" product contains un-geolocated decoded IR counts. The level 1.5 browse image products are sub-sampled "postage stamp" BT images designed for quick-look facilities. The accuracy of the ATSR 1 km data is of order 0.5°K, but problems which have been noted and under ongoing investigation are:

a) The co-location of the dual and single fields in the SST products often produce images with a "record grooving" effect due to the interpolation of a greater area into the 1 km^2 cells.
b) There is some evidence that contamination of data by the onboard cooler electronics has occurred.
c) The 3.7μm channel ceased to function after May 1992.

A summary of the ATSR data held at JRC is shown below:

Region	Start Date	End Date	No. SST products	No. of BT products	Latitude Start-End	Longitude Start-End
Bellings-hausen Sea	15.04.92	08.10.92	751	751	50S to 70S	65W to 90W
SWINDEX-Agulhas	14.04.92	03.10.92	2189	678	20S to 62S	2W to 30E
Drake Passage	19.04.92	15.08.92	69	69	50S-55S	65W to 90W
Azores	04.03.92	01.11.93	107		38N to 29N	21W to 31W
Western Med.	04.03.92	01.11.92	173	66	29N to 45N	10E to 40E

Low Spatial Resolution Data

The spatially averaged ATSR data (ASST) is of high quality. Some data for individual orbits within the North Atlantic are on exabyte at the JRC, but the most useful set of data is the global set of 0.5° latitude/longitude data for the period between August 1991 to December 1993. However, the data for August 1991 to December 1991 is of poor quality. A copy of the data set held at RAL is on erasable optical disk (JRC900) at JRC. A monthly subset of this data that has been subjected to various quality controls at JRC exists in on-line storage as well.

AVHRR Data

High Spatial Resolution Data

High spatial resolution (~1 km^2) AVHRR data exists (255 passes) on exabyte for the North Atlantic region over the period 26/04/91 to 31/08/91. A further 29 passes over the regions of Europe, Northeast Atlantic and the Mediterranean are also on exabyte. These data are stored on exabyte in Dundee format and can be read using the DSP software.

Low Spatial Resolution Data

A global set of multi-channel sea surface temperature (MCSST) data as produced by the Rosenstiel School of Marine and Atmospheric Sciences (University of Miami) exists on exabyte at the JRC. The data is for the period between November 1981 to September 1992. The data has a nominal spatial resolution of ~18 km at the equator. For more information on the data format see Smith (1992) and for information on the quality of MCSST data see the overview of MCSST data in Appendix A.

Data Storage

Currently the JRC has the following volumes of satellite IR SST data on exabyte tapes:

DATA	Number of Exabyte Tapes	Gigabytes
AVHRR High Resolution	14	12
AVHRR Low Resolution	2	9
ATSR High Resolution	62	24

2.3 Inventory of altimeter data

The datasets to be used in this project are from ERS-1 (launched in July 1991), TOPEX/POSEIDON (T/P) (August 1992) and ERS-2 (launched in April 1995). The altimeters on ERS-1 and T/P have functioned extremely well so far and the data are of high quality. Several forms of ERS-1 and T/P data have been acquired by JRC (see below) but for this project analysis will concentrate on the Off-line Precision Records (OPR).

Satellite/Data type	Start date	End date
ERS-1 FD	28 Dec 91	30 June 93
ERS-1 OPR	12 Aug 91	26 Oct 93
ERS-1 IGDR	26 Nov 91	6 Dec 94
T/P GDR	23 Sept 92	1 Apr 94
T/P IGDR	23 Sept 92	29 Apr 93

2.4 Inventory of scatterometer data

The only satellite scatterometers operating within the time frame of the project are those on ERS-1 and ERS-2. After problems with its calibration and with testing and selection of wind algorithms ERS-1 data of comparable quality to Seasat are now being distributed. Again, there are several versions.

Satellite/Data type	Start date	End date
ERS-1 FD	1 July 92	28 Feb 94
ERS-1 Freilich	25 Nov 91	28 March 94
ERS-1 IFREMER	2 March 92	30 June 93
ERS-1 I-PAF	1 July 93	31 Aug 93

CHAPTER 3. PRELIMINARY ASSESSMENT OF PRIORITIES

Based on the preceding inventory we are now well placed to make a preliminary assessment of priorities. One could argue that it would be most profitable to focus initial attention on *in situ* data sets which have been acquired with high resolution in the upper ocean, i.e. those containing both SeaSoar and ADCP data. Ocean structure below the thermocline is likely to be less strongly coupled to surface signatures of dynamic topography and, particularly, SST. Favoured cruise data sets would therefore include CD51 (Iceland-Faeroes Front), Sterna (Drake Passage and Bellingshausen Sea) and the two SWINDEX cruises (South West Indian Ocean). If successful when applied to such cases, methods for extrapolating surface and near-surface data to even deeper layers could be tested utilising full-depth CTD sections (A23 and SWINDEX II, for example).

Cases of coincident hydrography/altimetry are also likely to yield useful results (see Section 4.2). Future work will therefore also include analysis of CD66 (Azores region) and any follow-up cruises in this well-surveyed region of the North Atlantic subtropical gyre.

An early priority involves identification of significant mesoscale features in the satellite and/or cruise datasets. Considering satellite data alone, we expect to find instances where there are coincident signals in the SST and dynamic topography. However, depending on surface and meteorological conditions, we also expect to see examples where this is *not* so, e.g. when vertical coherence is disrupted by storms, thereby decoupling the upper ocean layers from deeper structure. In such a case, there may well be areas of strong SST signature but no associated dynamic height anomaly.

At a later stage we intend to follow two general approaches:

(a) incorporating satellite observations in inverse techniques in order to determine subsurface structure and circulation (Tokmakian, 1994),

(b) utilisation of empirical orthogonal functions (EOFs) and normal modes in order to extrapolate surface information to deeper layers as performed, for instance, in feature modelling (Heathershaw *et al*, 1993).

Maps of altimeter-derived dynamic topography may be scrutinised, via complex EOF analysis and Hovmoller diagrams, for evidence of propagating Rossby and Kelvin waves (Tokmakian and Challenor, 1993). Such propagating energy is often linked to subsurface oceanic adjustment related to changes in wind stress or instabilities resulting from influx of water from another region, and may have a corresponding signature in hydrodynamic data.

Satellite observations may also shed light on the subsurface dynamics of the ventilated thermocline: potential vorticity of deeper layers is set by the wind stress curl at the surface outcrop location. Scatterometer data, together with altimeter data, could yield a surface signature which is strongly tied to the subsurface circulation at considerable depths.

CHAPTER 4. PROGRESS ON SUB-PROJECTS

4.1 Sub-project 1: analysis of coincident *in situ*, altimetry and infrared data

4.1.1 TOPEX/POSEIDON altimetry in the South Atlantic

The South Atlantic is a relatively unsurveyed region, and thus lends itself well to study by remote sensing. 16 months of TOPEX/POSEIDON altimeter data have been analysed in the region 80° W - 40° E, 70° S - 10° N. The processing techniques used and results obtained are described below.

Processing

Standard altimetric corrections were applied to the altimeter sea surface height ($\overline{SSH}$) above a reference ellipsoid: dry tropospheric, wet tropospheric and ionospheric (dual frequency for TOPEX DORIS for POSEIDON) corrections. The Cartwright and Ray tidal model was used to remove tidal signals, and points shallower than 2000m were eliminated (to avoid contamination of the data due to tidal model deficiencies). The inverse barometer correction and the NASA sea state bias correction were also applied. A host of rejection criteria were employed to eliminate bad quality data. To obtain a

time series of data at known points, a reference grid was defined using the sub-satellite track givenby cycle 18, since this is the closest cycle to the nominal cycle . Data were collocated onto this reference grid using a perpendicular bisector approach to eliminate along-track mean sea surface slope. The Rapp Mean Sea Surface model was used to correct for across-track slope. (This approach can prevent significant errors (~10 cm) occurring in regions of high mean sea surface slope. e.g. South Sandwich Trench).

The corrected data were averaged, giving a mean SSH at each point on the reference grid, for the period 23/9/92-10/2/94. The standard deviation of the SSH variability was also obtained, and is shown in Figure 1. The OSU91A geoid was subtracted from the mean SSH to look at the large-scale low-frequency circulation.

The mean SSH was then subtracted from the SSH for each cycle, to obtain height anomaly fields for each cycle. Thus, the geoid and low frequency SSH variation is eliminated. Height residual profiles for particular tracks were examined, and clear biases of the order 10 cm could be seen. This is thought to be residual radial orbit error, and a bias+cosine model, with a period of one orbit revolution was fitted to each track and residuals calculated to eliminate this source of error. The resulting fields give information about the mesoscale circulation.

Results

Large Scale Circulation:

Subtracting the geoid from the mean SSH to obtain sea surface topography is limited by the accuracy of the geoid which is well known only on large scales. Hence, the resulting picture (Figure 2) is one where the large scale features can be seen, for example the sub-tropical gyre, the Antarctic Circumpolar Current, and the Agulhas retroflection.

Mesoscale Circulation:

Features such as mesoscale eddies, and meanders of fronts can be seen in the height anomaly maps obtained by subtracting the 16 month mean SSH from each cycle. (For a typical example see Figure 3) In the Agulhas region eddies with a positive height signature (warm core) can be tracked moving into the centre of the South Atlantic, from the retroflection region. The problem with using T/P for this is that the distance between tracks is fairly large (315 km at the equator), and therefore the spatial resolution is poor and eddies 'fade' in and out of view.

Future Work:

Attempts are now underway to investigate the regions and times where there is a correlation between SST and SSH. For this purpose, the height residuals will be compared to ATSR SST residuals from an annual+semiannual model, the rational here being to compare like with like. This could pinpoint areas/times where the SST bears some relationship to the subsurface temperature.

4.1.2 Annual and Semiannual Variations of Satellite Derived Sea Surface Temperature in the North Atlantic

A decade of multi-channel SSTs derived from AVHRR in the form of a reduced volume data set (spatial resolution of ~18 km^2 at the equator and temporal resolution of one week) were further reduced to a 0.5° latitude by 0.5° longitude monthly data set. The derivation of the data and the quality of the MCSST data is discussed in Appendix A.

Data between August 1983 and September 1992 were screened for erroneous values derived from , land, sea, or cloud and were averaged into monthly 0.5° latitude by 0.5° longitude cells so long as there was at least two data points (2 one week averages) per cell.

One hundred and ten months of monthly mean SST values for each of the 181 by 181 grid cells were used to fit the linear model :

$$SST_t = a_0 + \sum_{j=1}^{2}\left[a_j \cos\left(\frac{2\pi jt}{12}\right) + b_j \sin\left(\frac{2\pi jt}{12}\right) + e_t \right]$$

where SST_t is the SST at month t (expressed in months after 1 January 1984), a_0 is the constant term, a_1 and a_2 are the estimated regression coefficients for the most significant harmonic, b_1 and b_2 are the regression coefficients for the least significant harmonic, and e_t is the error term assumed to be independent and normally distributed. The model was fitted only if there were 12 months or more of data. An F-test was used to determine the significance of the annual and semiannual components at the 95% level. The method used was to fit the annual and semiannual models separately and if both were significant then the joint model was used with the most significant harmonic first, else only the results from the significant single model were used. Various results of the significant test are shown in Figure 4(c) where yellow indicates that both components were significant but the semiannual component was most significant, red indicates that both components were significant but the annual harmonic was most significant, green indicates that only the annual harmonic was significant, and blue indicates that only the semiannual component was significant. Figure 4(f) shows the percentage of the variance explained by the harmonic terms The amplitude of the annual and semiannual components are shown in Figures 4(a) and 4(b) and corresponding amplitudes in Figures 4(d) and 4(e) which show the period of maximum value (in days of year).

Figure 4(c) shows that over the majority of the North Atlantic the annual cycle is highly significant whereas the semiannual cycle is not. Where the semiannual cycle is significant it is less significant than the annual cycle, except for two regions: the Intertropical Convergence Zone (ITCZ) near the equator where the annual cycle is not significant, and a small region of the Labrador Sea where the semiannual cycle is more significant than the annual cycle. The highest SSTs are in the Gulf Stream region and to the west of it off Newfoundland, where local warming probably predominates. An interesting result is that the high annual amplitudes associated with the Gulf stream do not show further out into the Atlantic. Around this core region of high annual amplitude some scattered isolated "rings" are shown, especial to the south and northeast. These may represent the positions of persistent meanders in the Gulf Stream and this requires further study. The general trend in the phase of the annual amplitude is shown as a function of day of year from January 1st, and for the region north of the equator demonstrates that maximum amplitude occurs earliest in the north, only occurring in the subtropical gyre by October. The maximum amplitude is interpreted as marking the onset of seasonal (annual) cooling. At high northerly latitudes around Iceland, cooling begins in July and this follows a south-west to north-east tongue extending into the central Atlantic.

4.1.3 Investigation of the skin effect

Data from the SOFIA cruise, which occurred between 1 June and 20 June 1992 in a region near the Azores, has been used to calibrate and validate an experimental ship borne radiometer which was designed to measure the radiometric sea surface temperature(i.e. the SST emitted from the very surface micro layer). Present knowledge dictates that under most conditions (including those experienced during the cruise) conventionally measured, or bulk, SST (i.e. beneath the surface micro layer) is a few tenths of a degree (~0.5K) warmer than that of the top layer. This effect results from surface cooling caused by heat flux momentum (Robinson *et al.*, 1984)). This surface temperature difference ΔT is known as the skin temperature. The bulk SST was measured by a trailing thermistor and the end of a rope running along side the ship at a depth of ~1 cm. This data was calibrated against "Met. Office" type buckets taken periodically throughout the cruise.

The method chosen to calibrate the radiometric SST was to

(a) correct various constants (emissivity of sea water, emissivity of the reference black-body, instrument calibration coefficients) used in the processing of the data,

(b) to smooth out jumps in the internal calibration coefficients,

(c) to correct for contamination of the SST signal by reflected incoming longwave radiation by using measured incoming longwave radiation data to estimate the sky temperatures, and

(d) to add an additional error term to account for a warm bias in the data, so that the radiometric SST was under most conditions similar (but slightly cooler) than the measured bulk SST.

These improvements reduced the radiometric SST in the mean by 0.5K. The incorporation of the so-called heat source term (Thomas *et al.*, 1993) was the main contributor in the improved calibration, but it could also be interpreted as a correction for the fact that extrapolation from the internal black-body

calibrations is required owing to the fact that the sea temperature was nearly always colder than the "cold" black-body, rather than a correction for some extra (unknown) heat source within the radiometer.

Validation of the radiometric SST was performed by comparing the measured skin temperature difference with a modelled skin temperature (Hasse, 1971). This was done for night time instances, (see Figure 5) when incoming shortwave solar radiation could not contaminate the skin temperature difference, and showed there to be virtually no bias (0.01K) between the measured and estimated ΔT, as opposed to a 0.61K bias observed with the original radiometric SST data. However the slope of the regression is only 0.75, which indicate that the Hasse (1971) model is estimating too high by 25%.

Further investigation of deviances between the measured and estimated skin temperature difference show that as a function of incoming longwave radiation the two sets of data agree in trend. At night the model ΔT is larger in magnitude (cooler skin) than the observed ΔT. Whereas during the day the model ΔT is smaller in magnitude (warmer skin) than the observed ΔT at lower levels of incoming longwave radiation. This effect is mainly due to the model ΔT becoming larger in magnitude at night than during the day, while there is less change between the daytime and night-time observed ΔT, except for an increase in magnitude of night-time observed ΔT (relative to the daytime observed ΔT) concomitant with a decrease in the model daytime ΔT at lower levels of incoming longwave radiation during the day (see Figure 6). This is consistent with a comparison of measured and estimated ΔT against incoming short-wave radiation (Figure 7) which shows that at higher levels of solar radiation the measured ΔT is greater. This may suggest that at increasing levels of incoming shortwave radiation the radiometer is reading too low, or that the Hasse (1971) model does not estimate the shortwave radiation effect correctly, although this model is the only skin temperature model which takes into account the differential absorption of solar radiation at various depths. Another possibility is that the floating thermistor data was contaminated at these wave lengths, but there was no suggestion of this in the comparisons with the bucket temperatures.

4.2 Sub-project 2: Application and development of techniques for using satellite data to improve estimates of sub-surface information

4.2.1 Absolute Currents from Radar Altimetry

The major problem with oceanographic data from satellite altimeters is our ignorance of the geoid. This means that we have to use the altimetric mean sea surface as an estimate of the geoid and calculate all oceanographic parameters relative to this surface. The upshot of this is that any information on flow which is constant is confounded with the gravity signal and is thus impossible to separate. A method is presented here which uses *in situ* data to get around this problem and thus obtains mean currents from a combination of altimetry and hydrography (Challenor *et al.*, 1995) .

Some Theory

Let the height of the sea surface relative to the reference ellipsoid (as measured by the altimeter, assuming perfect corrections) be h.

Let the height of the sea surface relative to a Level of No Motion be H.

Since the geoid is parallel to a Level of No Motion the height of the geoid relative to the ellipsoid is given by

$$G \pm k = H_{t0} - h_{t0} \tag{1}$$

where k is an unknown constant and the subscript gives the time at which the measurements where taken.

Differentiating w.r.t. x (the direction along which the measurements are taken)

$$\frac{\partial G}{\partial x} = \frac{\partial H_{t0}}{\partial x} - \frac{\partial h_{t0}}{\partial x} \tag{2}$$

Since G is invariant with time

$$\frac{\partial H_t}{\partial x} = \frac{\partial H_{t0}}{\partial x} - \left(\frac{\partial h_{t0}}{\partial x} - \frac{\partial h_t}{\partial x} \right) \tag{3}$$

Thus we can calculate the along track slope of the sea surface relative to the geoid at time t from the altimeter measurement of surface height if we have simultaneous measurements of the sea surface height relative to a Level of No Motion and the altimeter.

From geostrophy

$$\frac{\partial H_t}{\partial x} = \frac{f v_t}{g} \tag{4}$$

where v_t is the geostrophic current, f is the Coriolis parameter and g is the acceleration due to gravity.

$$\therefore v_t = v_{t0} - \frac{g}{f}\left(\frac{\partial h_{t0}}{\partial x} - \frac{\partial h_t}{\partial x}\right) \tag{5}$$

Therefore if measure the surface geostrophic current simultaneously with an altimeter pass we can estimate the surface current at any time the altimeter takes a measurement along the same track.

Application

So far we have applied this method in two areas: the Drake Passage and the Azores:

Drake Passage

In November 1992 *RRS Discovery* sailed from the Falkland Islands to Elephant Island across Drake Passage as part of the Sterna Cruise. This part of the track is shown in Figure 8. The line followed is WOCE line SR1 and lies along an ERS-1 ascending track in the 35 day repeat phase of the mission. ERS-1 collected data along this track on day 314 of 1992. The ship moved south along the track from day 315 to 317. *Discovery* towed an undulating SeaSoar carrying a CTD and an Acoustic Doppler Current Profiler (ADCP). This was the first cruise to use the ASHTECH GPS 3DF system for obtaining the ship's heading for correcting the gyro error in the ADCP measurement.

ERS-1 traverses this pass every 35 days and data are so far available from days 174, 209, 244, 279, 314, and 349 of 1992 and day 18 of 1993. ERS-1 will stay in this orbit until the end of 1993 and both ERS-1 and ERS-2 should be in the same orbit at the beginning of 1995. Thus it should be able to monitor the flow through this part of the Drake Passage for 18 months with ERS-1 data and for 3-5 years with ERS-2 which is expected to stay in the same orbit for its entire operational lifetime.

Figure 9 shows the density field interpolated from the undulating SeaSoar profiles. Superimposed on the density contours is the bottom where this is less than 400 m. The important feature to note is the Burdwood Bank in the north of the section where the water is less than 150 m deep. This density field can be used to compute the geostrophic shear but not the velocity as we do not know the level of no motion. The ADCP however does measure a true velocity. At the surface this will include an ageostrophic component and thus cannot be compared to the geostrophic velocities computed from the altimeter. By matching the geostrophic and ADCP shears a 'Level of Known Motion' was found, at 198m. Surface geostrophic currents were then computed. Note that over the Burdwood Bank there is no level where the ADCP current is geostrophic and hence no surface geostrophic current can be produced.

After the usual corrections the ERS-1 data were corrected for orbit error by fitting a once per rev sine curve using data over the whole Southern Hemisphere. The sea surface heights were then differentiated to provide surface slopes. These were taken relative to the pass on day 314 (i.e. the slopes as measured on day 314 were subtracted from each pass) and converted into geostrophic velocities using (2). The resulting relative velocities are shown in Figure 10.

We now have velocities relative to day 314 from the altimeter and true velocities as measured by the ship at approximately the same time. Now we can add the relative currents to the current measured by the ship to obtain an absolute current from the altimeter every 35 days. These currents are shown in Figure 11.

There are a number of points on interest in this plot. The first is that there is a persistent banded structure to the currents with a zero or westward flow between 56.5° and 57.5°S. What appeared to be an eddy on the density plot is in fact part of this persistent structure. It is believed that this region of westward or zero flow is topographically forced.

Azores

In March-April 1992, a cruise was conducted by Robin Pingree of Plymouth Marine Laboratory on *RRS Charles Darwin*. The principal objectives were to examine winter mixing, subduction and phytoplankton production in the subtropical front. As depicted in Figure 12, one leg was planned along a ground track of ERS-1 in its first Ice Phase (3-day repeat mission). Seven CTD casts were made at intervals of 1 degree latitude. Absolute velocity measurements were collected using the ADCP. The geostrophic and ADCP velocity fields were matched to obtain an estimate of the absolute surface geostrophic current perpendicular to the ship's track .

By combining *in situ* data with the altimeter-derived currents relative to the day of ship passage (day 67), a plot of the time evolution of the absolute currents, at a nominal 3-day sampling interval, could be made (Figure 13). (Missing days were either not provided in the altimeter data set from NOAA, or did not satisfy certain quality control criteria for removal of orbit error). The Figure indicates significant variation in the structure of the currents on rapid time scales. (Gaps due to missing points in the altimeter data set are apparent). Overall, however, we find that the observed variability of the Azores Current is surprisingly small, in comparison with previous published hydrographic results.

ACKNOWLEDGEMENTS

Useful talks with many colleagues (too numerous to mention) both within, and outside, the James Rennell Centre are gratefully acknowledged.

REFERENCES

Bacon, S., 1994: An attempted proof that an inversion works: Convex-91 hydrographic results compared with ADCP measurements. Submitted to *J. Ocean. Atmos. Techn.*

Challenor, P. G., J. F. Read, R. T. Pollard, and R. T. Tokmakian, 1995: Measuring surface currents in the Drake Passage from altimetry and hydrography, *submitted to Journal of Physical Oceanography*.

Hasse, L. 1971. 'The Sea Surface Temperature deviation and the heat flow at the sea-air interface', *Boundary-Layer Meteorol.*, 1, 368-379.
Heathershaw, A.D., D.A. Smeed, S. Alderson and J.T. Allen, 1993: The Application of Feature Modelling in Ocean Forecast Systems and Critical Parameters. DRA report TM (USSF) 93116.

King, B. and S. Alderson, 1994: SR1 Repeat Hydrography/ADCP, Drake Passage, November 1993. *International WOCE Newsletter* , 15.

Robinson, I. S., Wells, N. and Charnock, H. 1984. 'The sea surface thermal boundary layer and its relevance to the measurement of sea surface temperature by airborne and spaceborne radiometers', *International Journal of Remote Sensing*, 10, 19-45.

Smith, E. 1992. *A users guide to the NOAA Advanced Very High Resolution Radiometer Multichannel sea Surface Temperature data set*, Jet Propulsion Laboratory Physical Oceanography Distributed Active Archive Centre, California, 22 pp.

Thomas, J. P., Knight, R. J., Roscoe, H. K., Turner, J. and Symon, C. 1993. 'The Calibration of a Ship-borne Infra-red Radiometer for measuring sea surface temperatures', *Submitted to the Journal of Atmospheric and Oceanic Technology*,

Tokmakian, R.T., 1994: The Iceland-Faeroe Front: a Synergistic Study of Hydrography and Altimetry. *Journal of Physical Oceanography*, **24**, 2245-2262.

Tokmakian, R.T. and P.G. Challenor, 1993: Observations in the Canary Basin and the Azores frontal region using Geosat data. *J. Geophys. Res.*, **98(C3)**, 4761-4773.

Zavody, A. M., Gorman, M. R., Lee, D. J., Eccles, D., Mutlow, C. T. and Llewellyn-Jones, D. T. 1994. 'The ATSR Data Processing Scheme Developed for the EODC', *International Journal of Remote sensing*, **15**, 827-843.

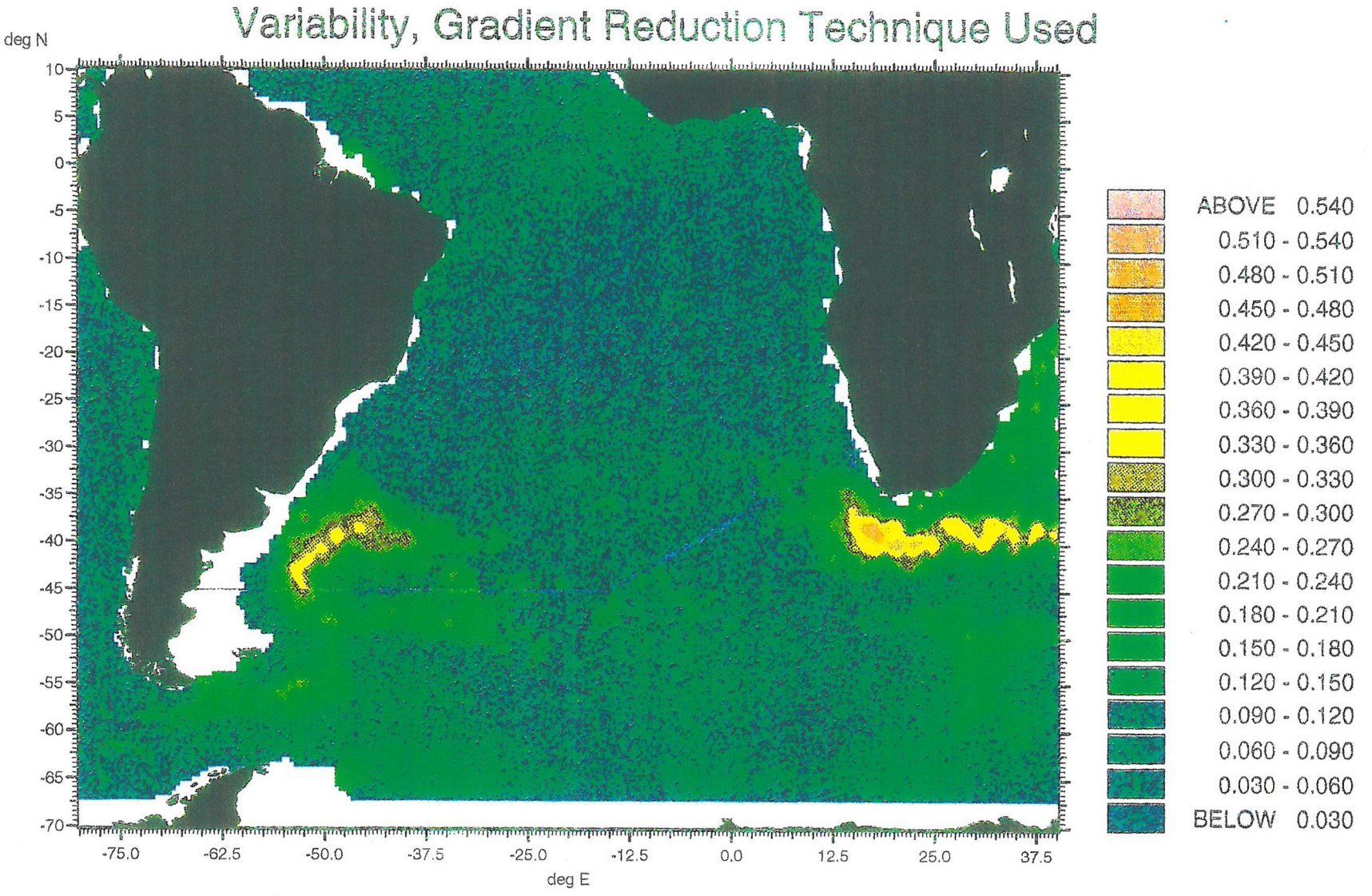

Figure 1. Variability of sea surface height of the South Atlantic between 23/9/92 - 10/2/94 as measured by Topex/Poseidon.

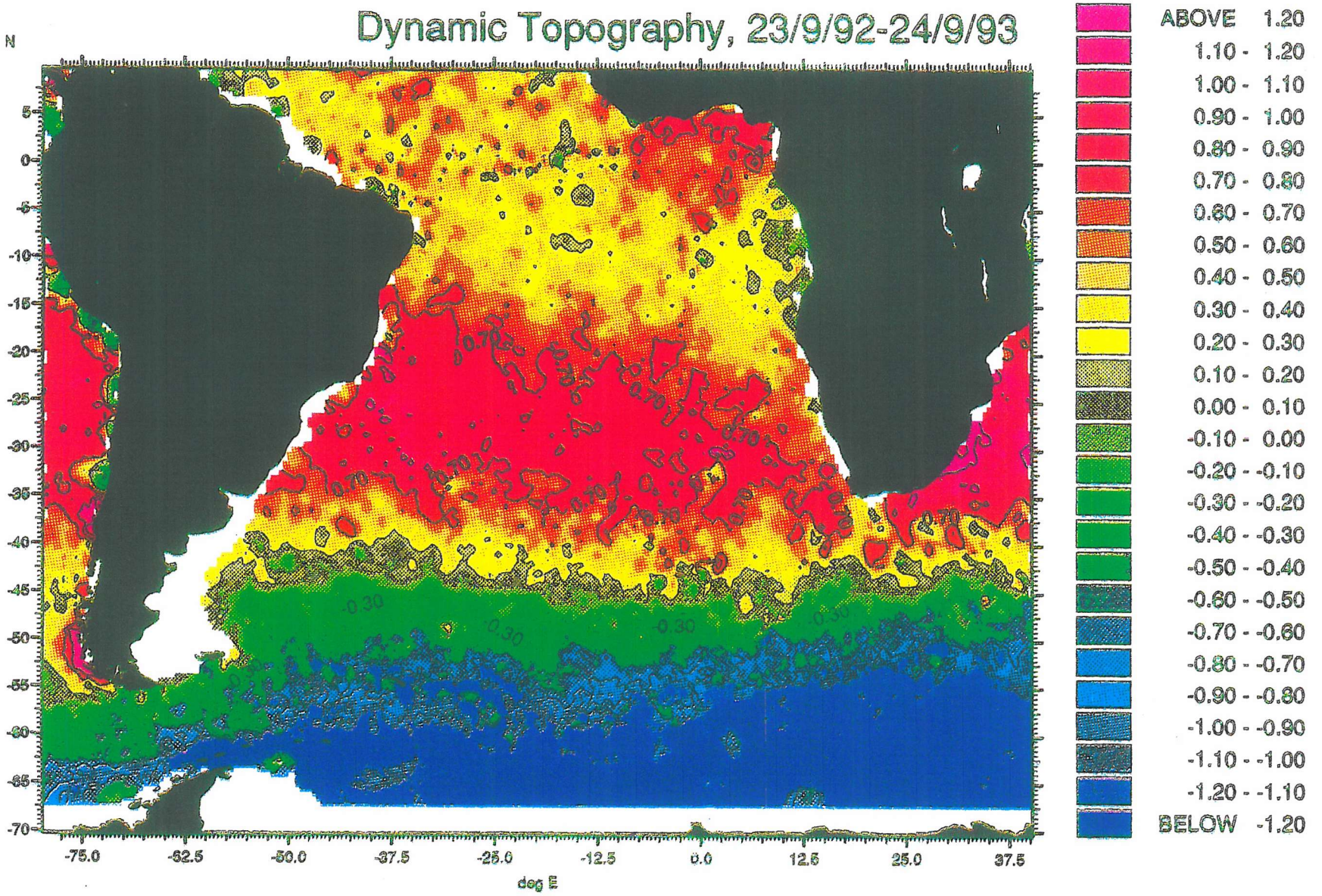

Figure 2. Large scale circulation of the South Atlantic as observed by Topex/Poseidon.

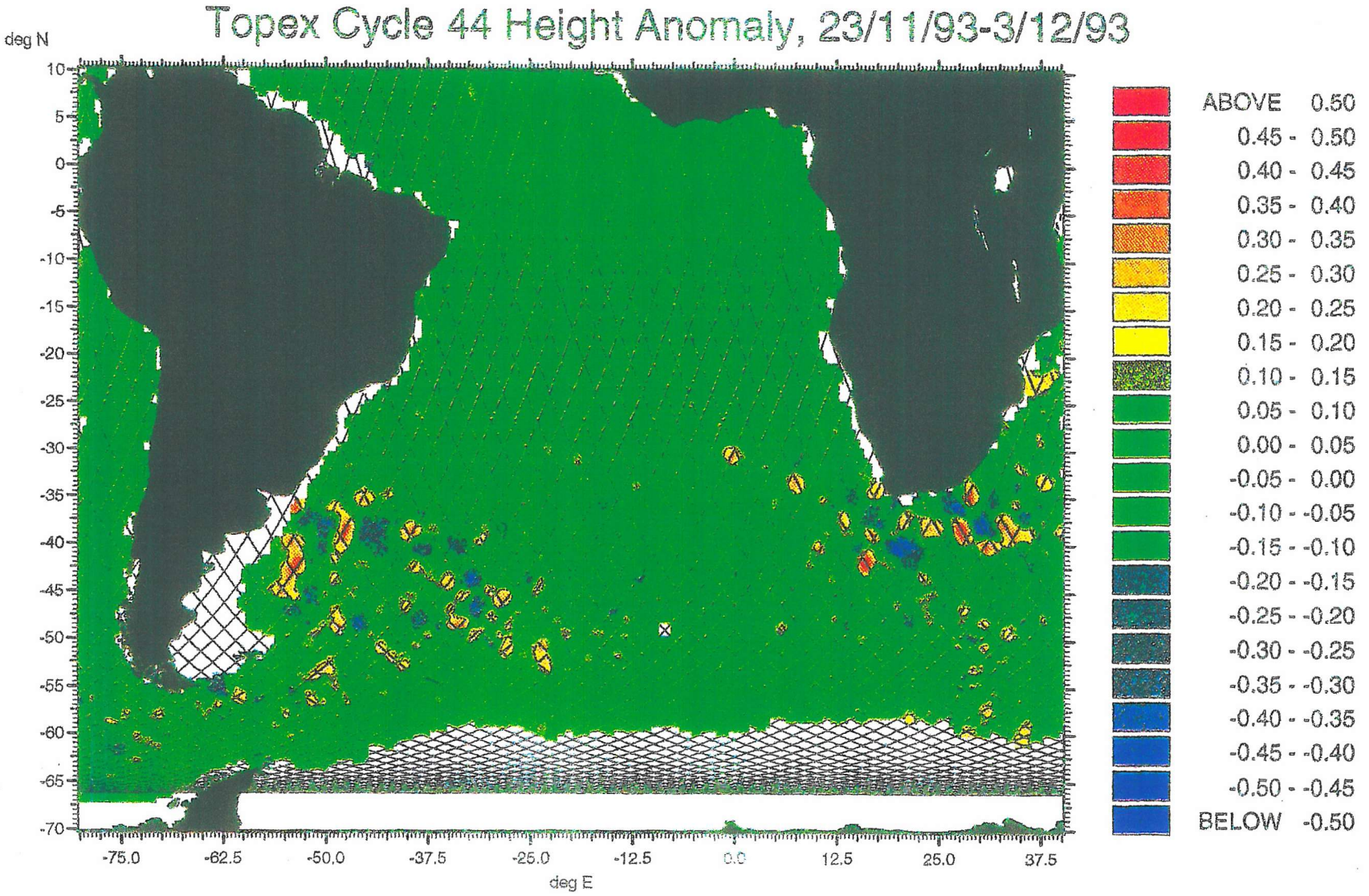

Figure 3. Mesoscale features in the South Atlantic observed by Topex for cycle 44.

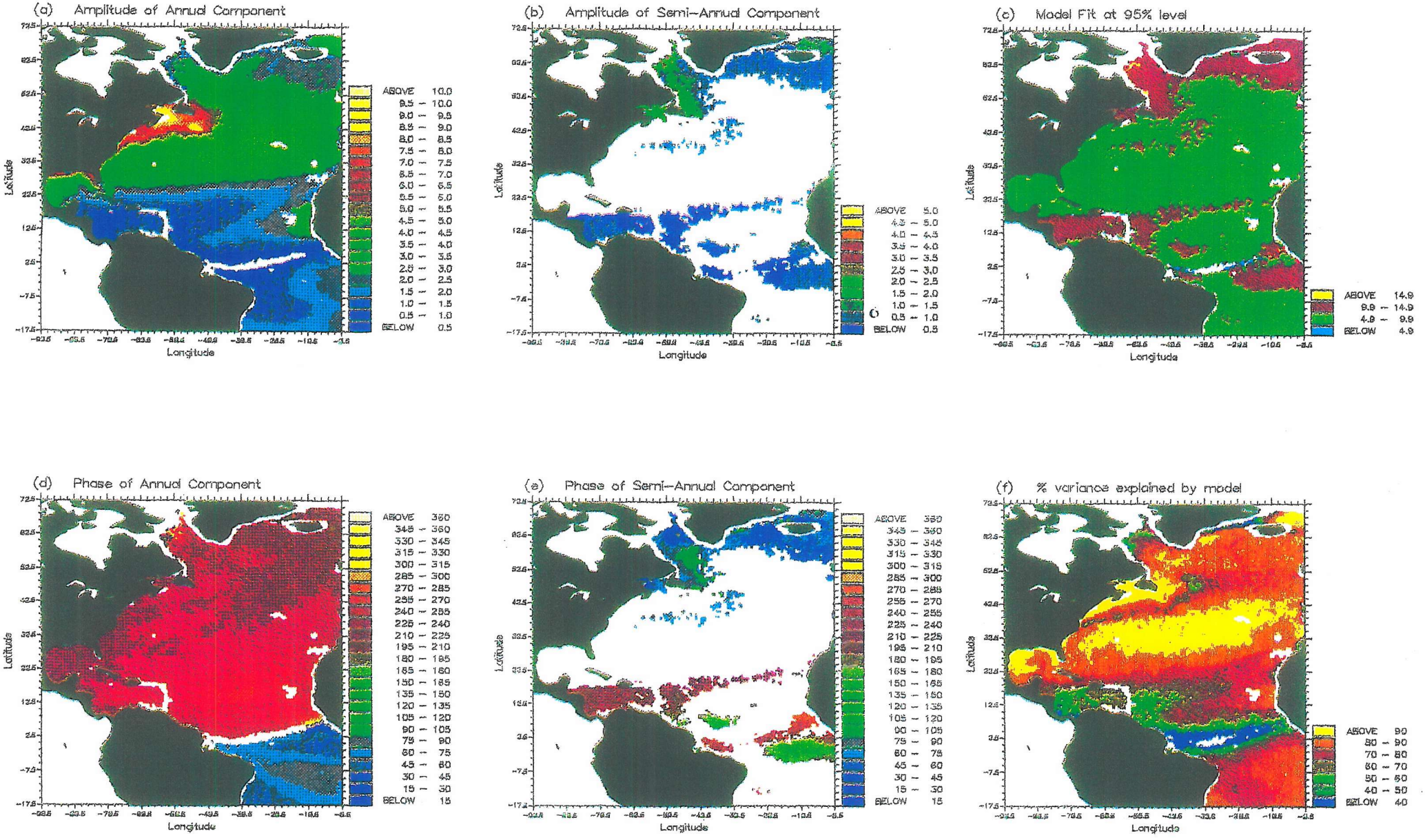

Figure 4. Analysis of monthly mean North Atlantic sea surface temperatures observed by AVHRR (see text for details).

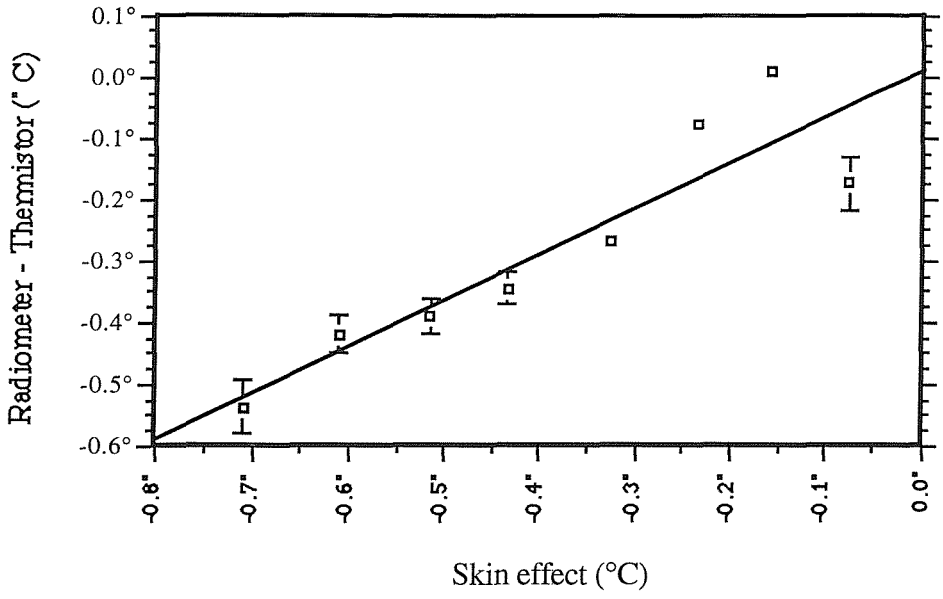

Figure 5. The difference between the reprocessed radiometer and trailing thermistor SST values plotted against the skin temperature. The ten minute mean SST data were averaged for 0.1°C increments of the skin effect using night time cases only where more than 10 data points occurred. The fitted line has the equation:

(radiometer - thermistor) = 0.01 + 0.75 (skin value), units in °C.

(a) daytime data

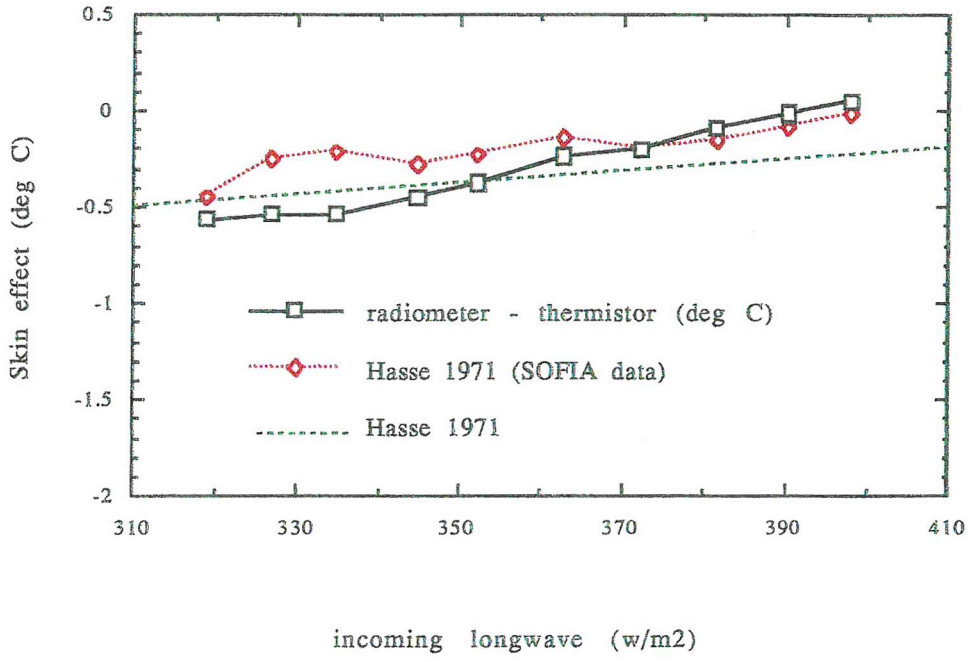

(b) night-time data

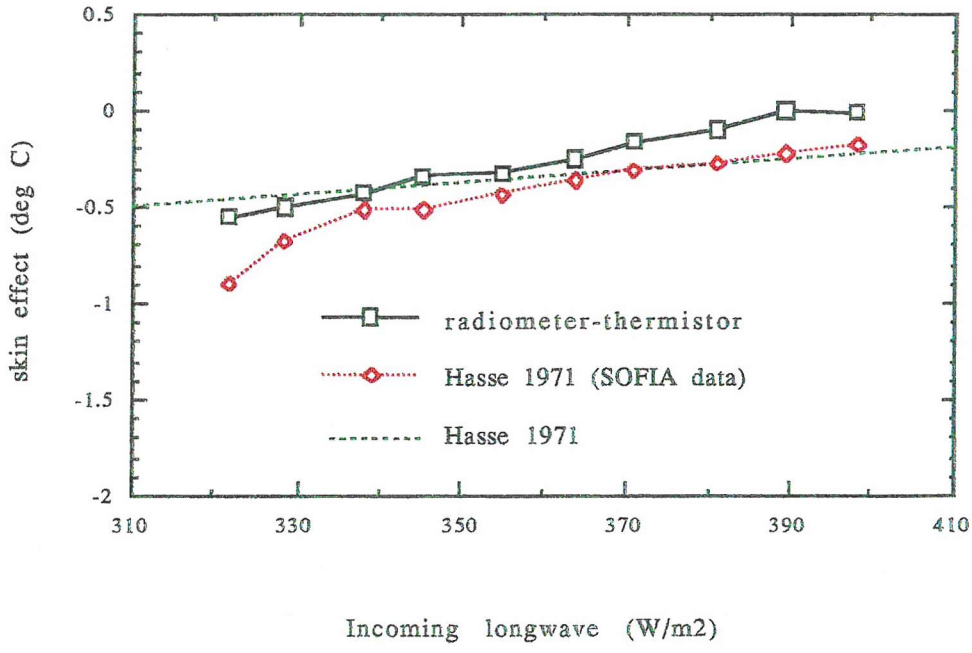

Figure 6. Observed skin effect variation with the incoming longwave radiation. The top figure is for daytime data and the bottom one for night-time data. Shown are the difference between the radiometer and thermistor values for SOFIA, and the skin effect calculated from the Hasse (1971) formula using the SOFIA meteorological observations. Also shown is the relationship between skin effect and turbulent heat flux used in the Hasse formula.

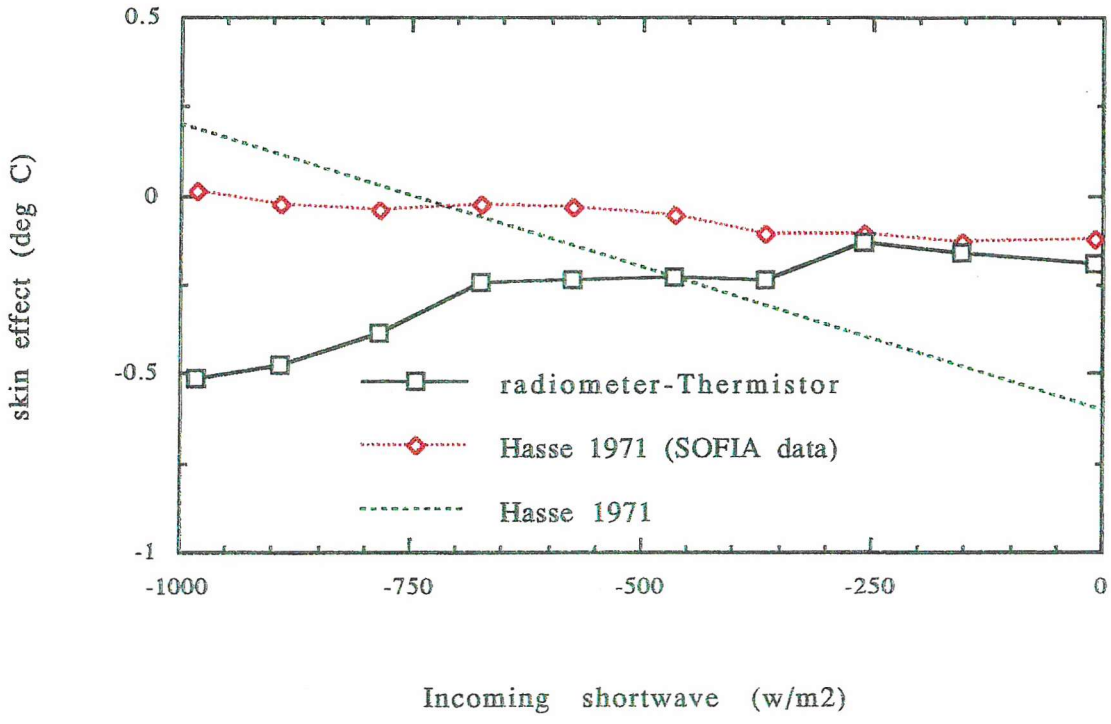

Figure 7 As Figure 6(a) but showing the variation with incoming shortwave flux.

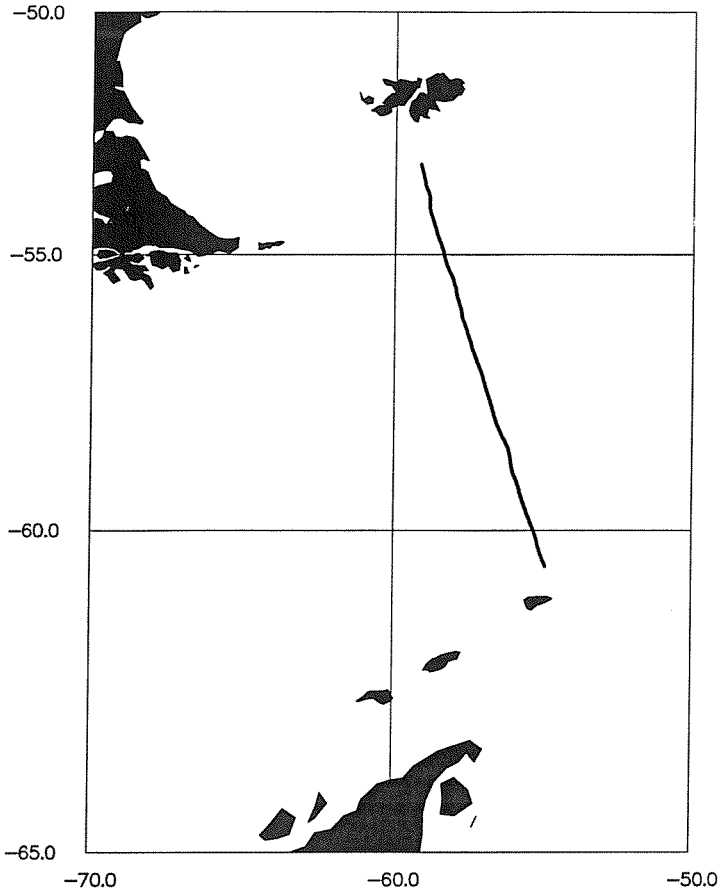

Figure 8. WOCE line SR1, lying along an ERS-1 ascending track across the Drake Passage, followed as part of the Sterna Cruise by *RRS Discovery* in November 1992.

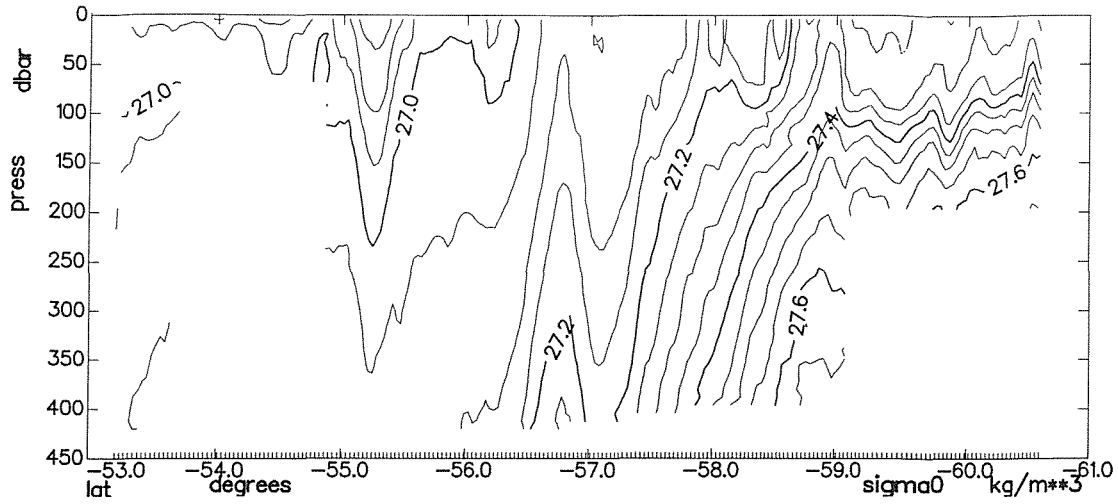

Figure 9. Density field across Drake Passage (see figure 8) as obtained from SeaSoar observations in the Sterna Cruise.

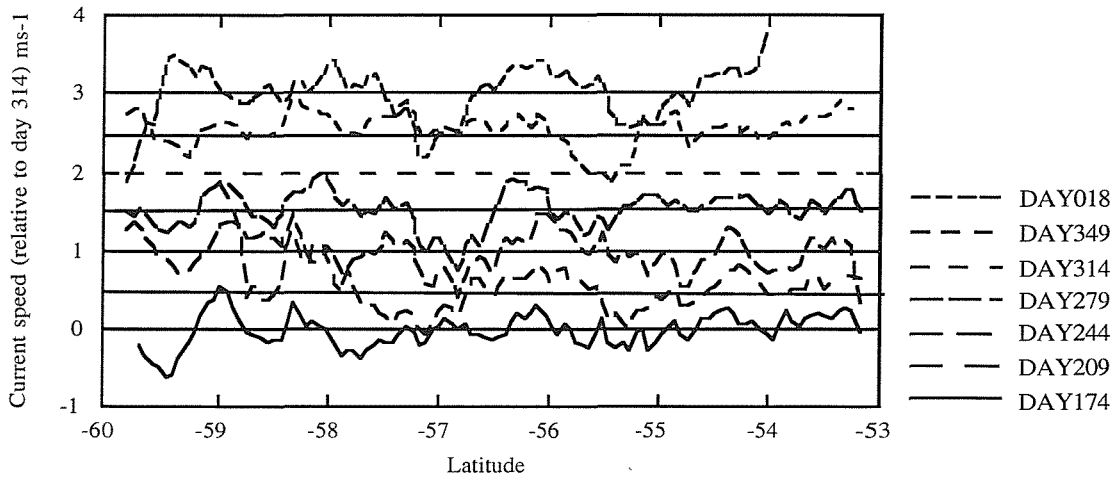

Figure 10. Current speeds relative to the altimeter pass on day 314 (each pass is offset by 0.5 m s^{-1}).

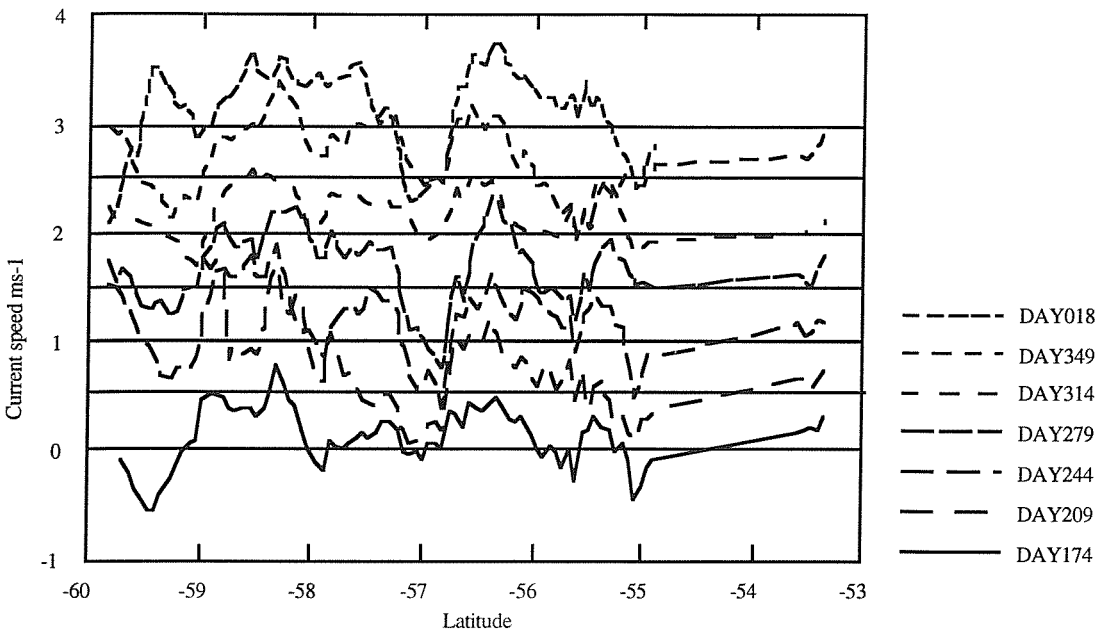

Figure 11. Absolute current speeds from a combination of altimetry and in situ data. Note the data gap over the Burdwood bank. Each pass is offset by 0.5 m s^{-1}.

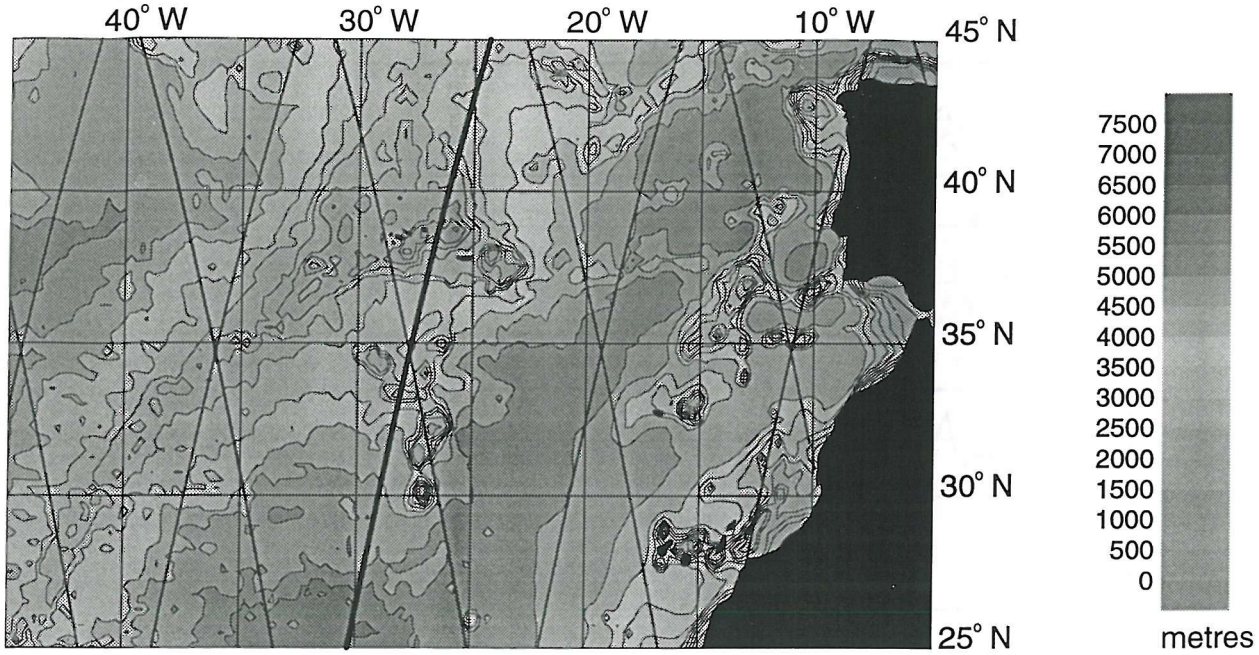

Figure 12. North East Atlantic Canary Basin and Azores Current region. The ground track pattern of ERS-1 in its 3-day repeat phases (Ice Phases B and D) are indicated. The highlighted track was sailed by RRS Charles Darwin between 37°N and 31°N on March 5 to March 7, 1992. The plot also shows the bathymetry. Part of the Mid-Atlantic Ridge can be seen extending from southwest to northeast in the western half of the map.

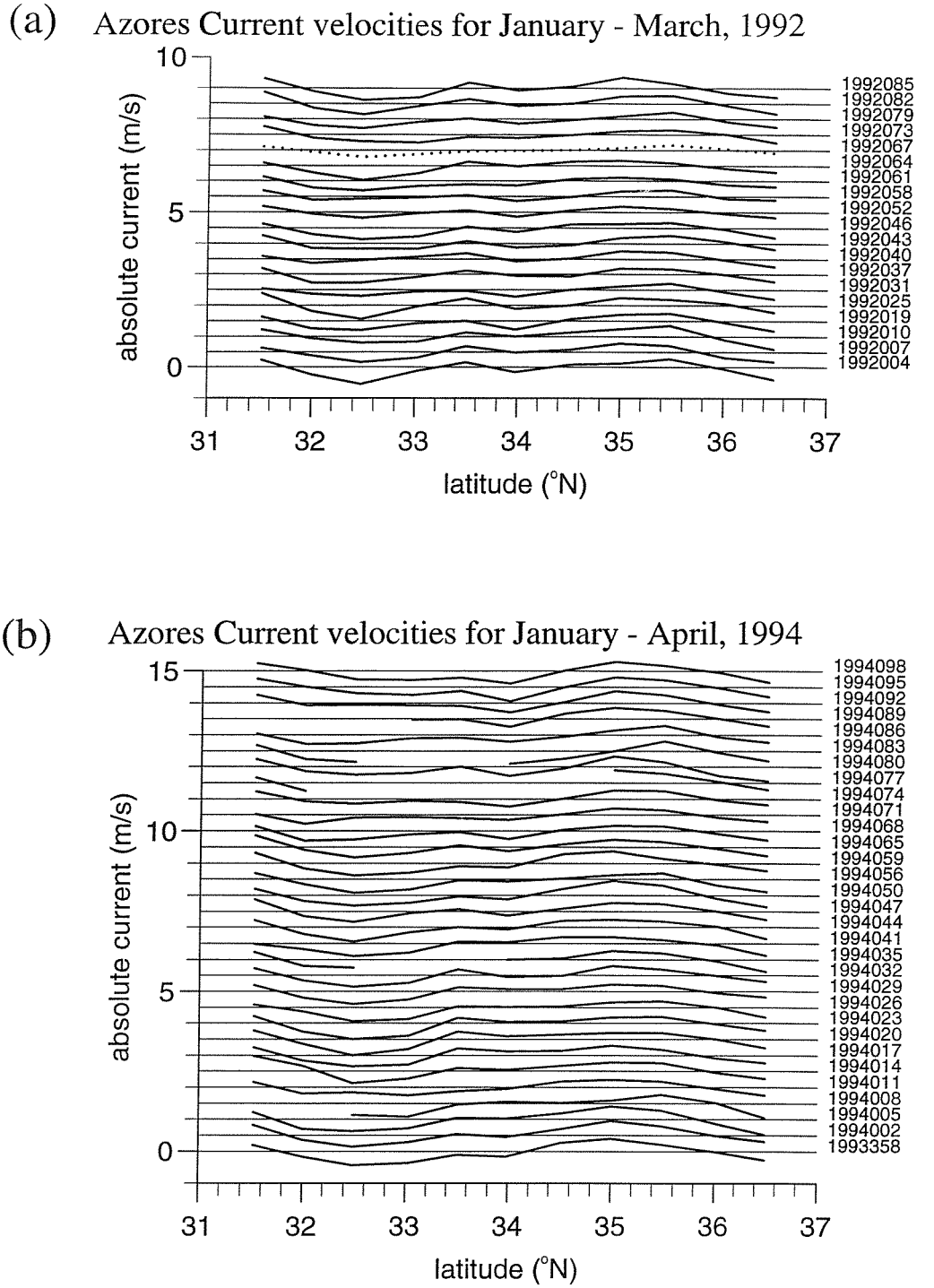

Figure 13. Profiles of cross-track absolute surface geostrophic current velocities for (a) ERS-1 Phase B (December 27, 1991 to March 30, 1992) and for (b) Phase D (December 23, 1993 to April 10, 1994). Seven-digit numbers at right indicate year and day number. The dotted current profile indicates the pass nearest to ship passage (1992067). Variability in position of the maximum velocity of the westward current lobe centred around 35°N can be seen.

APPENDIX A

Overview of MCSST Data

1. Reduced volume MCSST data sets

From the large primary NOAA/NESDIS MCSST data set several reduced volume data sets have been produced, for example in one product [*Strong*, 1991] all MCSST retrievals are binned into 2.5° by 2.5° latitude-longitude grid for each month. [*Bates and Diaz*, 1991] use the daily global MCSST analysis described above and bin this data into a 1° by 1° grid using the same processing techniques as described in the "Field analysis" section of [*McClain et al.*, 1985]. A third data set [*Halpern et al.*, 1992] and [*Halpern et al.*, 1991] is a monthly average of MCSSTs taken from a weekly average on a ~18 km by ~18 km grid produced at the University of Miami Rosenstiel School of Marine and Atmospheric Science RSMAS. This data set is described in more detail in section 3.

2. The NOAA/NESDIS MCSST data set

NOAA have operationally produced global SST products since January 1979, the first was the Global Operational Sea Surface Temperature Computation (GOSSTCOMP) from 1st January 1979 to 17th November 1981, the second was the Multi Channel Sea Surface Temperature (MCSST) from 17th November 1981 to 2nd March 1990 and the third the Cross Product Sea Surface Temperature (CPSST) from 2nd March 1990 until present. During any operational phase there are two NOAA satellites in use, one in a morning orbit (even numbered satellites) and one in an afternoon orbit (odd numbered satellites) with local equator crossing times of 7:30 am and 1:30 pm respectively. The main component of these global SST data sets is data from the Advanced Very High Resolution Radiometer (AVHRR). With the exception of GOSSTCOMP data all the other global SST data have only been derived from the odd numbered NOAA satellites because these satellites carry the AVHRR/2 instrument which has 5 spectral channels unlike the AVHRR (carried on even numbered satellites) which only has four spectral channels[*Pichel*, 1991]. The first satellite to carry the AVHRR was the TIROS-N satellite. This satellite and the next one in the series (NOAA-6) provided the GOSSTCOMP data, satellites NOAA-7, 9, and 11 provided the MCSST data and NOAA-11 is currently providing the CPSST data. Table 1 shows the periods when each satellite was in operational use.

Satellite	Start	End
TIROS-N	19.10.78	30.01.80
NOAA-6*	27.06.79	05.03.83
NOAA-7	24.08.81	01.02.85
NOAA-8†	06.03.83	21.06.84
NOAA-9	25.02.85	07.11.88
NOAA-10	17.11.86	31.09.91
NOAA-11	08.11.88	Present
NOAA-12	01.09.91	Present

Table 1. The periods during which each satellite was in operational use are indicated * reactivated between 03.07.84 to 01.07.85 to stand in for NOAA-8, † turned off between 21.06.84 to 01.07.85 due to primary oscillator problems [*Kidwell*, 1991].

The prime input to the MCSST data processing system is the sensor level 1b data [*Kidwell*, 1991], which has a spatial resolution of ~4 km (an onboard computer generates an average radiance for each channel from four 1.1 km elements within each non-overlapping group of five consecutive 1.1 km measurements along a scan). The major steps in the production of MCSST data are:

(1) Target construction; AVHRR data passing initial quality checks [*McClain et al.*, 1985] are input into an 11 by 11 "target array" of 4 km pixels centred on each High Resolution Infrared sounder (HIRS) view;
(2) Land masking;
(3) Cloud detection,
(4) The cloud free unit-array channel counts are averaged calibrated and corrected for calibration non-linearities in the response of the 11μm and 12μm channels[*Weinreb et al.*, 1990] to form 8 km resolution brightness temperature data;

(5) MCSST algorithms are applied to produce a SST product.

The algorithms include coefficients derived from comparisons of the initial SST with buoy data. Periodically as the buoy SST data set increases for each satellite the algorithms used are updated [*Kidwell*, 1991]. Thus the MCSSTs archived on the NESDIS global retrieval tapes represent the average SSTs within 8 km x 8 km areas, which would occur at 25 km intervals in a cloud free environment; (6) The number of MCSST retrievals actually saved per target array of 11 by 11 GAC spots varies between day and night and geographically, with more densely sampled areas in regions surrounding USA and other selected regions [*Kidwell*, 1991]. [*McClain et al.*, 1985] gives a detailed account of the various processes including the different cloud detection and MCSST algorithms used in this primary MCSST data set.

3. RSMAS MCSST data Set

The MCSST data set produced by the University of Miami Rosenstiel School of Marine and Atmospheric Science (RSMAS) was obtained from Jet Propulsion Laboratory Physical Oceanography Distributed Active Archive Centre (JPLPO.DAAC) in California. The data is derived from the NOAA/NESDIS Global Retrieval Tapes which contain MCSST retrievals with associated latitudes and longitudes. The MCSST values (day and night observations form separate products) are binned into a cylindrical equi-rectangular global grid 2048 (longitude) by 1024 (latitude) space elements (which at the equator have an approximate spatial resolution of 18 km). The origin of this grid is 90°N and 180°W. From this global set eight regional subsets of data are available, one of which is the North Atlantic and Gulf of Mexico regional data set, which was the one used in this study and which extended over a period of 10 years from October 1981 to March 1992. This 512 by 512 pixel subset with associated flags included a region bounded within latitude 17.3S to 72.5N and longitude 8.3W to 98.2 W. For each grid point the average of all MCSST measurements available for one week is included. Gaps in the data are interpolated using an iterative Laplacian relaxation technique until all such areas connected to valid observations are filled: extant SST estimates that encompass the data voids are fixed and used as boundary conditions; the previous bi-weekly first guess field is used as an initial estimate, which are then relaxed until Laplace's equation is satisfied. A region is flagged as cloudy if the data void exceeds 130 km in two dimensions [*Olson et al.*, 1988]. The interpolation also creates an ice mask using Nimbus-7 SMMR data. This mask is created using the minimal ice extent for both hemispheres and combining the months of March and September for 1984, 1985 and 1986. The mask is used as a numerical boundary for the interpolation and attracts values towards -1.8°C. The minimal ice extent mask includes those areas that are always covered by ice [*Smith*, 1992].

4. Major Biases in MCSST DATA

[*Bates and Diaz*, 1991] compared MCSST data from 1989-1991 with the Comprehensive Ocean Atmosphere Data Set COADS [*Woodruff et al.*, 1987]. He found a maximum anomaly of 2°C in the spring of 1982 which was due to the injection of volcanic aerosols into the stratosphere associated with the eruption of El Chichõn, these biases extended latitudinally and biases of ~1°C remained throughout 1983. A series of eruptions of Mt. Pinatubo in late spring 1991 introduced immediate biases > 5°C [*Bates*, 1993]. NESDIS introduced new CPSST coefficients in October 1991, which improved the accuracy but biases of between ~0.5-1.0°C remained in the tropics. A change in the cloud thresholds used and a further eruption in late 1991 introduced another significant bias in the data over the southern hemisphere [*Bates*, 1993].

The use of the wrong calibration tables for AVHRR/2 (NOAA-9) in the first half of 1987 introduced zonally symmetric biases which are positive at brightness temperatures above ~288K and negative below this [*Bates*, 1993] and [*Bates and Diaz*, 1991]. Table 2 shows the major events which have affected the performance of the MCSST data set from the point of inception.

Date-start	Date-end	Nature of problem	Reference
1983		Failure of Ch4 & Ch5	
04.11.81		Period RSMAS MCSST data for this study	
01.01.79	17.11.81	GOSSTCOMP data set	Pichel 1991
24.11.81		Changed precision of MCSST day algorithm	Kidwell 1986
01.04.82*	30.12.84*	Mt. El-Chichon volcanic aerosol contamination	Bates & Diaz 1991
01.07.82*	01.02.85*	Ch3 Noise (poor accuracy)	Pichel 1991
15.09.82		Intro. volcano triple window SST	Kidwell 1986
13.10.82		Ch3 really noisy	Kidwell 1986
12.10.83		Day & Night obs. compare well (end of El-chicon effect)	Kidwell 1986
08.11.83		Introduction of Viewing angle correction term	Bates & Diaz 1991
29.11.83		New Day MCSST	Kidwell 1986
13.12.83		Stopped Sargasso Sea High-density sampling	Kidwell 1986
05.01.85		NOAA-9 operational	Kidwell 1986
06.10.86		NL calibration tables introduced (ch4 ch5)	Bates & Diaz 1991
06.10.86	01.04.88*	Problems with NL calibration	Pichel 1991
01.12.86*	01.01.87*	Volcanic ash Kliuchevskoi Volcano	Bates & Diaz 1991
01.01.87*	01.06.87*	Miscalibration	Bates & Diaz 1991
28.10.88		Triple Window Night	Bates & Diaz 1991
01.03.90*		Introduction of CPSST	Pichel 1991
01.06.91*		Mt. Pinatubo volcanic aerosol contamination	Bates 1993
01.10.91*		NESDIS introduce new coefficients for Mt. Pinatubo correction, this was partially successful	Bates 1993

Table 2, Major events effecting the accuracy of MCSST data, * means that there is some uncertainty of the actual day within the month specified.

References

Bates, J. J., A decade of multispectral sea surface temperature observations from space, *Adv. in Space Res.*, , 1993.

Bates, J. J., and H. F. Diaz, Evaluation Of Multichannel Sea Surface Temperature Product Quality for Climate Monitoring: 1982-1988, *J. Geophys. Res., 96(C11)*, 20613-20622, 1991.

Halpern, D., V. Zlotnicki, J. Newman, O. Brown, and F. Wentz, An atlas of monthly mean distributions of GEOSAT sea surface height, SSMI surface wind speed, AVHRR/2 sea surface temperatures, and ECMWF surface wind components during 1988., *91-8*, 110 pp., Jet Propulsion Laboratory, 1991.

Halpern, D., V. Zlotnicki, J. Newman, D. Dixon, O. Brown, and F. Wentz, An atlas of monthly mean distributions of GEOSAT sea surface height, SSMI surface wind speed, AVHRR/2 sea surface temperatures, and ECMWF surface wind components during 1987., *92-3*, 111 pp., Jet Propulsion Laboratory, 1992.

Kidwell, K. B., NOAA Polar orbiter Data Users guide, 230 pp., National Environmental satellite Data and Information service, 1991.

McClain, E. P., W. G. Pichel, and C. C. Walton, Comparative Performance Of AVHRR-Based MultiChannel Sea Surface Temperatures, *J. Geophys. Res., 90(C6)*, 11587-11601, 1985.

Olson, D. B., G. P. Podesta, R. H. Evans, and O. B. Brown, Temporal variation in separation of Brazil and Malvinas Currents, *Deep Sea research, 35*, 1971 to 1990, 1988.

Pichel, W. G., Operational Production of Multichannel sea Surface Temperatures From NOAA Polar Satellite AVHRR Data, in *Palaeogeography, Palaeoclimatology, Palaeoecology*, pp. 173-177, Elsevier Science Publishers B.V., Amsterdam, 1991.

Smith, E., A users guide to the NOAA Advanced Very High Resolution Radiometer Multichannel sea Surface Temperature data set, 22 pp., Jet Propulsion Laboratory Physical Oceanography Distributed Active Archive Centre, 1992.

Strong, A. E., Large-scale satellite-observed SSTs during the 1980s as compared with conventional SSTs, paper presented at the AMS 2nd Symposium on Climate Change, New Orleans, January 14-19 1991, 1991.

Weinreb, M., G. Hamilton, and S. Brown, Nonlinearity corrections in calibration of Advanced Very High Resolution Radiometer infrared Channels, *J. Geophys. Res.*, *95*, 7381-7388, 1990.
Woodruff, S. D., R. J. Slutz, R. L. Jenne, and P. M. Steurer, A Comprehensive Ocean-atmosphere data set., *Bulletin of American meteorological Society*, *68*, 1239-1250, 1987.

Cruise	Date	Area	Data	Comments
future:				
A23	Mar-95	S. Atlantic	full-depth CTD, ADCP, met.	North and south segments planned along altimeter ground tracks
SWINDEX II	7 Jan/21 Feb-95	S.W. Indian Ocean	moorings, full-depth CTD, SeaSoar, ADCP	Survey of Agulhas Return Current
past:				Leg(s) planned along Topex/Poseidon and/or ERS-1(2) ground tracks
ADOX II	Feb/Mar-94	Southern Ocean	moorings, full-depth CTD, ADCP	One short leg along Topex/Poseidon track
JCR	Nov-93	Drake Passage	full-depth CTD, XBT, ADCP	Drake Passage leg (as in Sterna cruise): WOCE line SR1
SWINDEX I (D201)	23 Mar/3 May-93	S.W. Indian Ocean	moorings, full-depth CTD, SeaSoar, ADCP,	Survey of ACC as it interacts with the Crozet Plateau
			XBT's	
ADOX I (D200)	6 Feb/18 Mar-93	Southern Ocean	moorings, full-depth CTD, ADCP	Study of flow of Antarctic Bottom Water from Weddell Sea into Indian Ocean
A11 (D199)	22 Dec-92/1 Feb-93	South Atlantic	full-depth CTD, XBT's, ADCP	WOCE hydrographic line along 45 S
Sterna (D198)	11 Nov/17 Dec-92	Southern Ocean	SeaSoar, ADCP, CTD, XBT's	Drake Passage leg along ERS-1 ground track in 35-day repeat mission
TEMPO	91 - 93	Tyrrhenian Sea	CTD, XBT, met.,satellite	Series of cruises
CD66	4 Mar/6 Apr-92	Azores	full-depth CTD, ADCP, limited SeaSoar,	One cruise leg along ERS-1 ground track in 3-day repeat mission
			XBT, moorings	
CD62a	6 Sep/28 Sep 91	Iceland-Faeroes	CTD, XBT,ADCP, met, sat., buoy	Two cruise legs along ERS-1 ground tracks (3-day commissioning phase)
CD62 (CONVEX)	1 Aug/4 Sep 91	N.E. Atlantic	full-depth CTD, XBT, met	Study of deep circulation and water masses
CD58&59 (Vivaldi)	25 Apr/10 Jun-91	N.E. Atlantic	full-depth CTD, SeaSoar, met.	Study of seasonal & interannual variations; heat & fresh water; eddies
CD51	24 Jul/21 Aug-91	Iceland-Faeroes	CTD, XBT, SeaSoar, ADCP, met	Included three small scale surveys of evolving eddy structure of the IFF.
D165a	Feb-87	Agulhas Current	moorings, full-depth CTD, SeaSoar, ADCP	Study of currents in the Agulhas retroflection region.
FASINEX	Feb/Mar-86	Gulf Stream	SeaSoar, CTD, AVHRR	Detailed study of Gulf Stream frontal region

Abbreviations:

ADOX: Antarctic Deep Outflow Experiment

CD: RRS Charles Darwin

CONVEX: CONtrol Volume EXperiment

D: RRS Discovery

FASINEX: Frontal Air-Sea Interaction Experiment

IFF: Iceland-Faeroes Front

TEMPO: Tyrrhenian Eddy Multi-Platform Observations Experiment


Natural
Environment
Research
Council